Histone Lysine Crotonylation Regulates Long-Term Memory Storage

Utsav Mukherjee[1,2,3], Budhaditya Basu[1,2], Stacy E. Beyer[1,2], Saaman Ghodsi[1,2], Nathan Robillard[1,2], Yann Vanrobaeys[1,2,4], Eric B. Taylor[5,6], Ted Abel[1,2*], and Snehajyoti Chatterjee[1,2*]

[1]Department of Neuroscience and Pharmacology, Carver College of Medicine, University of Iowa, Iowa City, IA 52242, United States

[2]Iowa Neuroscience Institute, University of Iowa, Iowa City, IA 52242, United States

[3]Interdisciplinary Graduate Program in Neuroscience, University of Iowa, Iowa City, IA 52242, United States

[4]Interdisciplinary Graduate Program in Genetics, University of Iowa, Iowa City, IA 52242, United States

[5]Fraternal Order of Eagles Diabetes Research Center, University of Iowa, Iowa City, IA 52242, United States

[6]Department of Molecular Physiology and Biophysics, Carver College of Medicine, University of Iowa, Iowa City, IA, 52242, United States

[*]Corresponding authors: ted-abel@uiowa.edu and snehajyoti-chatterjee@uiowa.edu

Keywords: crotonylation, hippocampus, long-term memory, gene expression, acylation

Running title: Novel histone acylation drives memory storage.

Abstract

Histone post-translational modifications (PTMs), particularly lysine acetylation (Kac), are critical epigenetic regulators of gene transcription underlying long-term memory consolidation. Beyond Kac, several other non-acetyl acylations have been identified, but their role in memory consolidation remains unknown. Here, we demonstrate histone lysine crotonylation (Kcr) as a key molecular switch of hippocampal memory storage. Spatial memory training induces distinct spatiotemporal patterns of Kcr induction in the dorsal hippocampus of mice. Through genetic and pharmacological manipulations, we show that reducing hippocampal Kcr levels impairs long-term memory, while increasing Kcr enhances memory. Utilizing single-nuclei multiomics, we delineate that Kcr enhancement during memory consolidation activates transcription of genes involved in neurotransmission and synaptic function within hippocampal excitatory neurons. Cell-cell communication analysis further inferred that Kcr enhancement strengthens glutamatergic signaling within principal hippocampal neurons. Our findings establish Kcr as a novel epigenetic mechanism governing memory consolidation and provide a foundation for therapeutic strategies targeting memory-related disorders.

Introduction

Precise spatiotemporal patterns of gene expression in the hippocampus are critical for the consolidation of long-term spatial memory (*1-4*). Histone PTMs play a key role in the epigenetic regulation of gene expression during memory consolidation (*5-9*). Short-chain acyl modifications on histone lysine residues are well-known PTMs that regulate several biological processes (*10-12*). Among these acyl modifications, histone lysine acetylation (Kac) has been extensively studied for its role in memory storage. Altering histone Kac levels by selectively manipulating the expression or function of 'writers' (lysine acetyltransferases, KATs) and 'erasers' (lysine deacetylases, KDACs) of histone Kac has been shown to impact hippocampal memory storage (*6, 13, 14*). Interestingly, recent evidence has shown that the majority of the writers and erasers for histone Kac also can also mediate the incorporation or removal of non-acetyl acyl moieties on histone lysine residues that structurally differ from the acetyl functional group (*15, 16*). This raises the question of whether the impact of KATs and KDACs on memory storage, as demonstrated in previous studies (*17-21*), also reflects underlying changes in non-acetyl histone acylations. Understanding the functional relevance of non-acetyl acylations in long-term memory storage will broaden conceptual insight into the epigenetic mechanisms underlying memory consolidation.

Although mechanistically and functionally distinct from Kac (*22*), lysine crotonylation (Kcr) can be regulated by the same writers and erasers that regulate Kac. Emerging evidence has revealed that lysine crotonylation (Kcr) plays a pivotal role in transcriptional regulation (*22-28*). Studies in cell-free systems have demonstrated that p300/CBP-mediated histone crotonylation activates transcription to a significantly higher extent than histone acetylation (*15*). Additionally, Kcr has been shown to be enriched on active gene promoters (*22*), and Kcr-mediated transcriptional regulation has been implicated in diverse biological functions, including as DNA damage repair (*23*), acute kidney injury (*27*), spermatogenesis (*24*), nerve-injury-induced-neuropathic pain (*28*), and neural stem cell differentiation (*25*). Interestingly, specific 'reader' proteins, such as the YEATS domain-containing proteins, exhibit a higher binding affinity for crotonylated lysine residues compared to acetylated lysine moieties (*29, 30*). The critical role of gene expression during hippocampal memory consolidation is well-established (*4, 31-33*). Yet, it remains unclear whether histone Kcr has a role in epigenetically regulating transcription during memory consolidation. In addition to writers and erasers, histone Kac and histone Kcr share enzymes that synthesize their respective metabolic precursors. The enzyme Acetyl-CoA synthetase 2 (ACSS2) synthesizes both crotonyl-CoA and acetyl-CoA (*15, 34*). ACSS2 plays a prominent role in long-term memory consolidation by regulating histone Kac-dependent gene transcription (*35, 36*). The role of ACSS2 in regulating Kcr-dependent gene expression has been

reported. However, it remains unknown whether the metabolic coupling of histone Kcr with gene transcription has a functional relevance in long-term memory consolidation.

Here, we provide evidence demonstrating the role of Kcr in hippocampal memory consolidation. We show that spatial learning in mice increases Kcr levels in the dorsal hippocampus during the early temporal window of memory consolidation. Next, we show that increasing histone Kcr levels by oral administration of crotonate, a precursor of crotonyl-CoA, enhances hippocampus-dependent long-term memory. Conversely, depleting histone Kcr levels in the hippocampus by overexpressing the crotonyl-CoA hydratase CDYL leads to long-term spatial memory impairments. We further show that enhancement of long-term memory by crotonate administration is regulated by the function of ACSS2. Utilizing single-nuclei transcriptomic and chromatin accessibility studies, we define unique molecular signatures of Kcr regulation across hippocampal subregions, demonstrating the impact of Kcr enhancement on genes encoding key proteins that regulate synaptic transmission and function. Our findings establish Kcr as a critical molecular switch that regulates hippocampal memory storage.

Results

Crotonylation is correlated with higher levels of activity-dependent gene expression.

We began with a bioinformatic analysis to determine the relationship between activating Kcr and Kac marks and activity-dependent gene expression in neurons. Histone crotonylation and acetylation share the same set of writers and erasers. Additionally, ACSS2 functions to synthesize the precursors for both acetylation (acetyl-CoA) and crotonylation (crotonyl-CoA). Because of this, we examined the correlation between activity-dependent gene expression, ACSS2, Kac, and Kcr enrichment on gene promoters by analyzing previously published chromatin immunoprecipitation followed by sequencing (ChIP-Seq) datasets (*15, 35, 37*). We found 2,340 gene promoters that show enrichment of ACSS2 and histone H3K27ac**,** while 2,239 gene promoters exhibit enrichment for ACSS2, H3K27ac, and H3K18cr **(Fig 1a)**. Next, we utilized a published dataset of activity-responsive gene expression (*2*) to compare the fold induction of genes enriched with ACSS2 and H3K27ac to genes enriched with ACSS2, H3K27ac and H3K18cr. Our analyses revealed that genes enriched with ACSS2, H3K27ac, and H3K18cr exhibit a significantly higher fold change compared to genes enriched with ACSS2 and H3K27ac **(Fig 1b)**. These results demonstrate that the presence of histone Kcr on gene promoters significantly heightens the magnitude of activity-induced gene expression, as found in studies of transcriptional regulation *in vitro* (*15*).

Spatial training induces lysine crotonylation in discrete hippocampal subregions.

To investigate whether training leads to changes in histone Kcr, we trained wild-type (WT) mice in a spatial object recognition (SOR) task and examined Kcr levels in core histones extracted from the dorsal hippocampus at specific intervals (0.5, 1, and 2 hr) post training (**Fig. 1c**). In the absence of prior knowledge regarding specific histone lysine residues affected by learning, we focused on pan-lysine crotonylation (Kcr) to assess the global landscape of histone Kcr during spatial memory consolidation. Using an antibody that detects crotonylated lysine residues, we observed that histone Kcr levels significantly increased at the one-hour timepoint after SOR training and returned to baseline levels at the two-hour timepoint (**Fig. 1d-e**). Next, we performed immunofluorescence using the Kcr antibody to investigate where Kcr levels increase in the hippocampus following training. Quantitative analysis of the nuclear Kcr levels revealed significant increases in the CA1 pyramidal cell layer, the subiculum, and the upper blade of dentate gyrus (DG) one-hour after spatial training, whereas no significant changes in the nuclear Kcr levels were observed in hippocampal subregions CA3 and the lower blade of DG (**Fig. 1f-h**). Taken together, these results identify histone Kcr as a novel epigenetic modification that exhibits distinct spatiotemporal dynamics in response to hippocampus-dependent training.

Reduction of hippocampal Kcr levels impairs long-term spatial memory.

The crotonyl-CoA hydratase Chromodomain Y-like protein (CDYL) is the only known regulator of Kcr that does not affect Kac levels. CDYL hydrolyzes crotonyl-CoA to beta-hydroxy butyryl-CoA (**Fig. 2a**), resulting in a reduction of histone Kcr levels (*26*). Interestingly, neuronal activity has been shown to reduce CDYL levels (*38*), prompting us to investigate whether spatial learning would similarly impact hippocampal CDYL levels. We performed immunofluorescence on brain sections obtained from SOR-trained WT mice to examine spatial patterns of learning-induced CDYL levels across hippocampal subregions (**Fig. 2b**). Hippocampal subregions CA1, subiculum, and the upper blade of DG exhibited significant downregulation of nuclear CDYL levels one-hour after SOR training, whereas nuclear CDYL levels remained unchanged in the hippocampal subregions CA3 and the lower blade of DG (**Fig. 2c-f).**

Next, to determine whether histone Kcr has a role in hippocampal long-term memory, we designed a strategy to selectively modulate Kcr in the dorsal hippocampus by manipulating levels of CDYL. We injected an adeno-associated virus (AAV) in WT mice to overexpress CDYL (AAV_9-CaMKIIα-CDYL-V5) in the excitatory neurons of the dorsal hippocampus (**Fig. 2g**). Immunofluorescence performed two weeks after viral infusion confirmed the expression of CDYL-V5 across the dorsal hippocampal principal layers (**Fig. 2h**). We observed significantly reduced Kcr levels in the hippocampal areas CA1 and CA3 in CDYL-V5-expressing mice compared to EGFP controls (**Fig. 2i-j**), thus validating the efficacy of our viral-based approach. Next, we evaluated long-term spatial memory in mice infused with

AAV-CDYL-V5 in the dorsal hippocampus. Mice were trained in the SOR task with objects that were placed in specific spatial locations within an arena. To test for long-term spatial memory, we performed a retention task 24 hr later with one of the objects displaced to a novel spatial location (**Fig. 2k**). Control AAV-infused mice (AAV_9-CaMKIIα-EGFP) exhibited a higher preference towards the displaced object during the test session, suggesting intact memory consolidation. Conversely, CDYL-infused mice (AAV_9-CaMKIIα-CDYL-V5) failed to exhibit any preference towards the displaced object during the test session (**Fig. 2l**). These results demonstrate that reduced levels of Kcr in the dorsal hippocampus leads to deficits in long-term spatial memory. Collectively, these findings suggest a critical role of hippocampal Kcr in spatial memory consolidation.

Pharmacologically increasing Kcr enhances long-term spatial memory.

Given that a reduction in hippocampal Kcr levels significantly impairs long-term memory, we next asked whether increasing Kcr levels could enhance long-term memory. Administration of crotonate, a short-chain fatty acid, has been shown to increase levels of histone Kcr (*15, 25*) and stimulate gene expression (*25*). Therefore, we implemented this strategy to pharmacologically increase histone Kcr levels in mice. We administered two different doses of crotonate (50 and 200 mg/kg) to WT mice by oral gavage and examined histone Kcr levels in the dorsal hippocampus one-hour after drug administration. We observed a significant increase in histone Kcr following 200 mg/kg dose of crotonate, whereas the 50 mg/kg dose of crotonate failed to enhance histone Kcr levels compared to vehicle (saline)-treated mice (**Fig. 3a-b**). Next, to study the impact of upregulating histone Kcr levels on long-term memory, we trained WT mice in a weak-learning (sub-threshold) SOR paradigm (*39*) to evaluate long-term memory enhancement. Mice were administered 50mg/kg of crotonate, 200 mg/kg of crotonate, or vehicle via oral gavage immediately after the completion of the training session. When tested 24 hr later, both the vehicle-treated and 50 mg/kg crotonate-treated mice failed to show a preference towards the displaced object, whereas mice administered with 200 mg/kg crotonate showed a significant preference towards the displaced object (**Fig. 3c**). Consistent with our SOR findings, we observed a significantly enhanced freezing response upon crotonate administration when mice were tested in a sub-threshold contextual fear conditioning (CFC) task (**Fig. 3d**). Our behavioral findings suggest that increases in histone Kcr levels improve hippocampal long-term spatial memory, further underscoring the functional relevance of Kcr for long-term memory. Additionally, our findings offer a conceptual framework for developing novel pharmaco-epigenetic strategies to enhance hippocampal memory consolidation.

Neuronal ACSS2 is a key regulator of crotonate-mediated memory enhancement.

The metabolic enzyme ACSS2 is critical for long-term memory and previous work has focused on the role of this enzyme in generating acetyl-CoA. However, ACSS2 also synthesizes crotonyl-CoA from the short-chain fatty acid crotonate in mammalian cells (**Fig. 4a**) (*15*). This prompted us to investigate whether ACSS2 regulates the increases in histone Kcr and enhancements in memory seen after infusion of crotonate. We injected an AAV vector (AAV_9-CaMKIIα-Cre-EGFP) into the dorsal hippocampus of male $ACSS2^{f/f}$ mice (*40*) to achieve a conditional knockdown of ACSS2 expression in the excitatory pyramidal neurons of the dorsal hippocampus (**Fig. 4b**). Immunofluorescence performed on brain sections obtained from the ACSS2 conditional knockout mice (ACSS2 cKO mice; $ACSS2^{f/f}$:CaMKIIα-Cre-EGFP) revealed the expression of Cre across hippocampal subregions (**Fig. 4c**). Western blot analyses confirmed the downregulation of ACSS2 in the dorsal hippocampus of ACSS2 cKO mice (**Fig. 4d-e**). We then examined the impact of crotonate administration on histone Kcr levels in ACSS2 cKO mice. We administered crotonate (200 mg/kg) or vehicle (saline) via oral gavage immediately after a sub-threshold training session, and quantified histone Kcr levels in the dorsal hippocampus one-hour after training. We found that crotonate treatment failed to enhance hippocampal histone Kcr levels in ACSS2 cKO mice (**Fig. 4f-g**), despite administering a dose of crotonate (200 mg/kg) that was sufficient to induce histone Kcr levels in WT mice (**Fig. 3a-c**). As crotonate administration failed to enhance Kcr levels in ACSS2 cKO mice, we hypothesized that crotonate treatment would also fail to elicit long-term memory enhancement in ACSS2 cKO mice. To test this hypothesis, we trained ACSS2 cKO mice in a sub-threshold learning SOR paradigm, administered vehicle or crotonate (200 mg/kg) immediately after training, and examined their long-term memory 24 hours after training (**Fig. 4h**). Our behavioral assessment confirmed that crotonate treatment in ACSS2 cKO mice had no impact in long-term memory compared to the vehicle-treated group (**Fig. 4i**). Taken together, these results demonstrate that ACSS2 is critical in mediating the molecular impact of Kcr on memory consolidation.

Single nuclei multiomics reveals the molecular signatures of memory consolidation following increases in Kcr.

We implemented a single nuclei multiomics (snRNA-seq and snATAC-seq) strategy to elucidate the molecular mechanisms underlying crotonate-mediated memory enhancement. Mice were trained in SOR using a sub-threshold learning paradigm, and oral administration of crotonate (200 mg/kg) or vehicle (saline) was performed immediately after training, as described previously (**Fig. 3c**). One-hour after crotonate administration, the dorsal hippocampus was harvested, and nuclei were isolated for single nuclei multiomics (**Fig. 5a**). Cell type clustering identified well-distinguished clusters comprising excitatory and inhibitory neurons, as well as clusters representing non-neuronal cell populations (**Fig.**

5b-c). Excitatory neurons were further classified into CA1, CA3, subiculum (Sub), dentate gyrus, and excitatory cortical neurons based on cell-type-specific marker gene expression (**Fig. 5b-c**). Notably, crotonate and vehicle treatment groups exhibited the same clusters (**Supplementary Fig. 1**). Next, we performed differential gene expression (DEG) utilizing the snRNA data along with differential accessibility regions (DARs) on the chromatin from the snATAC data of each cluster, comparing crotonate and vehicle treated groups. For downstream analysis, we used the DEGs (FDR<0.05, and absolute $\log_2$ fold change > 0.2) that exhibited concordant DARs (FDR<0.05, and absolute $\log_2$ fold change > 0.2) across their promoter and gene body (**Fig. 5d, Supplemental table 1**). We found that excitatory neurons in the CA1 hippocampal area showed the highest number of genes impacted by crotonate, with 205 upregulated genes showing increased chromatin accessibility and 36 downregulated genes showing reduced chromatin accessibility (**Fig. 5d**). Other cell types that showed a strong impact of crotonate on gene expression and chromatin accessibility were excitatory neurons in CA3 (118 upregulated genes with increased chromatin accessibility and 44 downregulated genes with reduced chromatin accessibility), subiculum (53 upregulated genes with increased chromatin accessibility and 18 downregulated genes with reduced chromatin accessibility), and the DG (27 upregulated genes with increased chromatin accessibility and one downregulated gene with reduced chromatin accessibility) (**Fig. 5d**). In addition to the principal neuronal clusters (CA1, CA3, subiculum, and DG), our analysis identified discrete molecular changes in inhibitory neurons (11 upregulated genes with increased DARs and 3 downregulated genes with reduced DARs) (**Fig. 5d**). Among the non-neuronal cells, oligodendrocytes showed the highest number of overlapping DEGs and DARs (24 upregulated and 27 downregulated) (**Fig. 5d**). Notably, we found a significant correlation between differential gene expression profiles and differential chromatin accessibility in hippocampal subregions CA1 and CA3 (**Supplementary Fig. 2**). Since manipulation of Kcr levels selectively in excitatory neurons was found to impact long-term memory, our subsequent analyses focused on DEGs within the neuronal populations of CA1, CA3, subiculum, and DG that also exhibit DARs.

To better understand the impact of Kcr enhancement on the molecular signatures of principal neuronal sub-types in the dorsal hippocampus, we performed Gene Ontology (GO: Molecular Function) overrepresentation analysis to identify the pathways enriched among the DEGs with DARs following crotonate treatment. We found that crotonate treatment impacted the expression of genes that were predominantly associated with regulating neurotransmission and synaptic function across the cell clusters (**Fig. 5e-h)**. Among the most significant pathways found enriched following crotonate administration, cell adhesion molecule binding was commonly enriched in subregions CA1, CA3, and subiculum, whereas distinct pathways attributed to ion channel activity were commonly enriched in CA1

and CA3 (**Fig. 5e-h, Supplemental table 2**). In contrast, pathways attributed to PDZ domain binding and calcium-dependent phospholipid binding were found enriched in the subiculum, whereas DG exhibited an enrichment of pathways related to protein kinase C activity and serine/threonine Kinase activity. (**Fig. 5e-h**). Because we found shared pathways between the principal neuronal subtypes of the hippocampus, we next investigated the genes commonly altered within these subregions. Utilizing an Upset plot, we compared unique and overlapping upregulated genes with concordant DARs in each cell-type. We found that CA1, CA3, subiculum, and DG showed a common upregulation of 2 genes (**Supplementary Fig. 3**). Notably, CA1, CA3, and subiculum showed 17 commonly upregulated genes, CA1, CA3, and DG showed a common upregulation of 4 genes, and CA1 and CA3 showed 22 commonly upregulated genes following crotonate treatment (**Supplementary Fig. 3**). Among the downregulated DEGs with reduced chromatin accessibility, we found pathways attributed to ephrin receptor activity, calcium ion transmembrane transporter activity, and phosphoric diester hydrolase activity downregulated in CA3, whereas pathways involved in cadherin binding and beta-catenin binding were downregulated in DG (**Supplementary Fig. 4**). We also identified 23 downregulated genes specific to CA1, 32 exclusively in CA3, and 12 selectively in the subiculum. Like the cell-type expression patterns observed with upregulated DEGs, there was some overlap in the expression of downregulated genes. Four genes were commonly downregulated across CA1, CA3, and the subiculum, while 8 downregulated genes were shared between CA1 and CA3 (**Supplementary Fig. 3**). To gain a mechanistic understanding of how crotonate-mediated changes in chromatin accessibility activate gene transcription, we performed a Transcription Factor Motif Enrichment analysis on the differentially accessible promoter regions of the upregulated DEGs (**Supplementary Fig. 4, Supplemental table 3**). Among the top 15 most significant TF motifs enriched on the promoters of upregulated DEGs across the cell clusters, TF motifs KLF15, ZNF148, and MAZ were found commonly enriched across subregions CA1, CA3, and subiculum (**Supplementary Fig. 4**). Additionally, we found TF motifs SP9, ZBTB14, SP3, and SP8 enriched on CA1 upregulated DEG promoters, TF motifs KLF16, ZNF740, ZBTB14 enriched on CA3 upregulated DEG promoters, and TF motifs SNAI2, RBPJ, and ZBTB33 enriched on the upregulated DEG promoters in subiculum. No significant TF motifs were found enriched in the upregulated DEGs in the DG. In summary, these findings indicate that Kcr plays a critical role in regulating the transcription of genes involved in synaptic function and neurotransmission within the principal excitatory neuron populations of the hippocampal circuit.

Cell-cell communication analysis reveals enhanced glutamate signaling following increases in Kcr

Activity-dependent synaptic transmission within the intrahippocampal circuit facilitates adaptive behaviors for encoding spatial, episodic, and contextual memories (*41-43*). Utilizing published databases of ligand-receptor interactions (*44*), we constructed an intercellular communication network of the principal neuronal subtypes to study the impact of Kcr enhancement on intrahippocampal signaling. Our analysis revealed that crotonate administration primarily increases the strength of glutamatergic signaling between the principal neuronal layers within the hippocampal circuit (**Fig. 6a**). Next, we investigated the ligand-receptor pairs in each intrahippocampal connection that exhibit increase in their communication probability following crotonate administration. We found that increasing Kcr levels strengthened the communication between distinct glutamatergic ligand-receptor pairs within specific neuronal networks of the hippocampal circuit. (**Fig. 6b**). These include the Slc1a2-Grik2/Grik4/Grik5, and Slc1a2-Gria4 pairs in the DG-CA3, Slc1a2-Grik2/Grik5/Grm7, and Slc1a1-Grik2/Grik5/Grm7 pairs in the CA3-CA1, and Slc1a1-Grik2/Grik5/Grm7, Slc1a2-Gria3/Gria4/Grik2/Grik5, and Slc17a7-Grik2/Gria3/Grm7/Grm8 pairs in the CA1-subiculum neuronal connection (**Fig. 6b**). We computed the communication probability of ligand-receptor interactions for glutamate signaling genes within principal neuronal cell types, which further confirmed the enhanced strength of glutamatergic transmission after crotonate treatment (**Fig. 6c**). Additionally, as proof of concept, we examined the expression levels of *Gria4*, one of the significantly upregulated genes involved in the glutamatergic signaling. Consistent with our single nuclei transcriptomic analysis (**Fig. 6d**), using RNAscope, we found a significant upregulation of *Gria4* in hippocampal subregions CA1 and subiculum following crotonate administration (**Fig. 6e-h**). Collectively, our findings suggest that a crotonate-dependent increase in histone Kcr augments glutamatergic neurotransmission within the hippocampal circuit.

Discussion

Epigenetic mechanisms, particularly histone acetylation, play important roles in memory consolidation (*6, 8, 13, 45*). In this study, we demonstrate the critical role of lysine crotonylation, an epigenetic mark associated with transcription activation (*10, 15, 29*), in modulating hippocampal long-term memory consolidation. Through pharmacological and genetic approaches, we demonstrate the bidirectional modulation of long-term memory by manipulating Kcr levels in the dorsal hippocampus. Mechanistically, our findings reveal that memory enhancement observed upon pharmacologically increasing Kcr levels is mediated through the function of ACSS2 to generate the precursor crotonyl-CoA in excitatory neurons in the hippocampus. Single-nuclei transcriptomic and epigenomic analysis further revealed that lysine crotonylation primarily regulates the chromatin accessibility and expression of genes linked to synaptic function and neurotransmission within principal neuronal populations in the

dorsal hippocampus. Our results identify a novel epigenetic mechanism underlying gene transcription during long-term memory storage.

Since the discovery of Kcr, researchers have been actively investigating the functional impact of Kcr on chromatin architecture and transcription, and several lines of investigation have reported key differences in the transcriptional regulatory mechanisms governed by histone Kcr compared to histone Kac. Firstly, the crotonyl group on histone Kcr has an extended hydrocarbon chain, making it bulkier and more hydrophobic than acetylation (*29, 30*). Such difference in the biophysical property of the crotonyl group potentially impacts the specificity of reader-Kcr interactions. Notably, YEATS domain proteins preferentially bind to Kcr by 2-7-fold compared to Kac (*30*), and the double PHD finger (DPF) domain of HAT complex MOZ-related factor (MORF) also preferentially binds Kcr over Kac (*46*). Secondly, biochemical studies have shown that histone Kcr-mediated transcriptional activation is stronger than acetylation (*15*), and that discrete Kcr marks promote gene expression through preferential recruitment of readers that interact with Kcr (*29*). Learning-induced gene expression and the epigenetic programs that regulate these transcriptional events are critical for long-term memory storage. Our findings establish histone Kcr as a critical epigenetic regulator of gene transcription during memory consolidation.

Histone acylation profiles are modulated by the nuclear concentrations of their respective metabolic precursor. We found that increasing crotonyl-CoA levels by administering crotonate in adult mice increased histone Kcr levels in the dorsal hippocampus and enhanced long-term memory. Conversely, depletion of crotonyl-CoA levels by overexpressing CDYL reduced histone Kcr levels and led to deficits in long-term memory. Together, these findings demonstrate the critical role of Kcr in regulating long-term memory storage and suggest that CDYL functions as a memory suppressor gene (*17*). Interestingly, we observed downregulation of nuclear CDYL protein levels after learning, providing a molecular explanation for the learning-responsive increase in nuclear Kcr levels observed in specific hippocampal sub-regions. Cellular levels of crotonyl-CoA are also regulated by the metabolic enzyme ACSS2, which synthesizes crotonyl-CoA from crotonate (*15, 34*). Recruitment of ACSS2 to transcriptionally active chromatin regions facilitates the transcription of memory-responsive genes (*35*), while whole-body knockdown or hippocampal silencing of ACSS2 results in long-term spatial memory deficits (*35, 36*). Crotonate fails to increase hippocampal histone Kcr levels or enhance long-term memory in ACSS2 cKO mice, indicating that ACSS2 is essential for maintaining the cellular pool of crotonyl-CoA. This finding also suggests that ACSS2 serves as a key metabolic regulator that links crotonate-dependent increases in Kcr levels with hippocampal memory consolidation. It has been hypothesized that different acyl-CoAs compete for binding to the KATs, supported by studies that

showed a marked increase in p300-dependent histone crotonylation upon depleting acetyl-CoA levels (*10, 15*). Thus, the nuclear concentration of crotonyl-CoA, and the abundance and activity of the enzymes that regulate crotonyl-CoA levels, are critical in regulating the epigenetic landscape of histone crotonylation during memory consolidation.

Alterations in synaptic architecture and adjustments in synaptic strength within the hippocampal tri-synaptic circuit (DG-CA3-CA1) facilitate memory consolidation (*47-49*). Our single-nuclei multiomics approach, aimed at elucidating the molecular underpinnings of Kcr-mediated hippocampal memory enhancement, revealed unique transcriptomic signatures within the hippocampal principal neurons. Our findings reveal that crotonate administration enhances gene expression and chromatin accessibility for genes related to glutamatergic neurotransmission, ion channel activity, and cell-cell adhesion within CA1 and CA3 hippocampal subregions. In particular, the upregulation of genes like *Grik2* in CA1 and *Grid2* in CA3 would be predicted to strengthen glutamatergic neurotransmission in these areas (*50-52*). Additionally, we observed Kcr-mediated upregulation of genes linked to the regulation of synapse development and circuit activity, such as *Kirrel3* in CA1, CA3 and subiculum, and *Nrxn2* in CA1 and CA3 (*53-55*). These genes related to cell adhesion function likely augment synaptic transmission dynamics between excitatory pyramidal neurons in the hippocampus circuit. Together, the differential upregulation of genes encoding key synaptic effector proteins indicates a mechanism that facilitates hippocampal long-term memory enhancement in response to increased levels of Kcr.

Cell-cell communication analysis from single-cell RNA-seq datasets has emerged as a powerful tool to infer and analyze intercellular communications between neuronal populations within defined circuits (*56*). Our analysis revealed that Kcr-enhancement augments glutamatergic neurotransmission through distinct glutamatergic ligand-receptor interactions within hippocampal connections. In the majority of these interactions, genes encoding for glutamate transporter genes, such as *Slc1a1*, *Slc1a2*, and *Slc17a7*, served as 'ligands'. *Slc1a1* and *Slc1a2*, encode Na^+-dependent excitatory amino acid transporters (EAATs) that mediate the clearance of extracellular glutamate in the extracellular space (*57, 58*), protecting hippocampal synapses from excessive glutamate receptor activation and neuronal excitotoxicity (*59, 60*). The *Slc17a7* transcript, encoding for the vesicular glutamate transporter 1 (VGLUT1), facilitates glutamate uptake into synaptic vesicles(*61*). The ‘receptor’ component of these ligand-pair interactions comprised primarily of distinct ionotropic kainate receptors (KARs), such as *Grik2*, *Grik4*, and *Grik5*, and AMPA receptors (AMPARs), such as *Gria4*. AMPARs mediate rapid excitatory synaptic transmission (*62*), while postsynaptic KARs suppress the slow afterhyperpolarization current during glutamatergic stimulation, leading to an increased action potential firing frequency at CA3-CA1 synapses (*63*). Additionally, KARs are known to bidirectionally modulate

the plasticity of synaptic AMPARs through non-canonical metabotropic signaling and PKC activation (*64, 65*). Thus, enhanced communication between the presynaptic EAATs and VGLUTs ('ligands') with the postsynaptic KARs and AMPARs ('receptors') potentially improves the dynamics and fidelity of glutamatergic neurotransmission within hippocampal circuit. Our findings provide unique mechanistic insights into the epigenetic regulation of glutamatergic neurotransmission and its implications in hippocampal long-term memory consolidation.

Intriguingly, most of the upregulated genes with increased chromatin accessibility following crotonate administration are not classical 'Immediate Early Genes' (IEGs) that act as markers of engram ensembles activated by learning in various spatial memory tasks (*4, 33, 66, 67*). Chromatin enrichment studies of histone Kcr have shown that an increase in histone Kcr correlates with a reduction in the transcription repressive mark (H3K27me3) and an increase in the transcription activation mark (H3K4me3), with no observed change in the occupancy of acetylated histones (H3K27ac)(*25*). Thus, increasing histone Kcr potentially enhances chromatin accessibility on bivalent gene promoters and activates their transcription without impacting the engram-specific IEGs that are likely to already exhibit an open chromatin conformation. The interplay of Kcr with other histone PTMs, such as acetylation and methylation, underscores the importance of the "histone code" underlying the regulation of gene expression during memory consolidation (*68, 69*). Recent studies have shown that histone Kac levels are a key determinant of engram activation and neuronal allocation into the fear memory trace (*70*), underscoring the importance of chromatin plasticity in memory encoding and synaptic remodeling. It remains to be investigated whether histone Kcr is also linked to the learning-induced activation of engrams and their integration into the spatial memory trace. Notably, gene expression signatures elicited by enhancing histone Kcr levels during memory consolidation are markedly different from the transcriptomic signatures elicited upon elevating histone acetylation (*71*), further suggesting that histone Kcr operates through a distinct mechanism in regulating hippocampal long-term memory.

While the strengths of our study stem from the conceptual novelty of our findings, several questions remain unanswered. Although we identify Kcr as a key regulator of long-term memory, further research is needed to pinpoint specific histone Kcr marks in the hippocampus induced by spatial learning and to determine whether these specific Kcr modifications are transcriptionally permissive. Additionally, because our pharmacological interventions to increase Kcr are not restricted to the hippocampus, it is possible that the observed long-term memory enhancement results from a combinatorial increase in Kcr levels across other brain regions. Another limitation is the lack of pharmacokinetic data regarding the administered drug in the mouse brain, and it is possible that optimal Kcr levels may be achieved at

a later time point beyond the 1-hr mark. Addressing these questions will provide valuable insights into the Kcr-mediated mechanisms that underlie long-term memory storage.

In summary, our work demonstrates the critical role of a novel histone acylation that has previously not been studied in the context of long-term memory. Our findings establish histone Kcr as a molecular switch for long-term memory, providing novel molecular insights into our conceptual understanding of epigenetic mechanisms that regulate long-term memory consolidation. We identified transcriptomic signatures of learning in distinct hippocampal subregions regulated by Kcr and emphasize the epigenetic control of glutamatergic neurotransmission as a critical mechanism underlying Kcr-dependent long-term memory enhancement. Given that recent studies have demonstrated the role of Kcr-mediated regulatory mechanisms in neurological disorders (*72, 73*), our work provides the conceptual framework to develop novel therapeutic interventions to treat brain disorders associated with cognitive impairment.

Methods

Data reporting: No statistical methods were applied to predetermine sample size.

***Mouse lines*:** Adult male C57BL/6J mice were purchased from Jackson Laboratories. The ACSS2$^{f/f}$ mice were generated at the University of Iowa Genome Editing Facility (*40*). This mouse model was created by inserting loxP sites flanking the Exon2 of ACSS2 using CRISPR/Cas9. The mice were 2-4 months of age at the time all the behavioral and biochemical experiments were performed. All mice had ad libitum access to food and water, and lights were maintained on a 12-hr light/dark cycle. All experiments were conducted according to US National Institutes of Health guidelines for animal care and use and approved by the Institutional Animal Care and Use Committee of the University of Iowa, Iowa.

Comparative analysis of activity-induced gene targets regulated by H3K18cr, ACSS2, and H3K27ac: We compared gene targets of H3K18cr in macrophages with gene promoters enriched with ACSS2 in the hippocampus and H3K27ac in the cortex. Raw sequencing data for each ChIP-seq dataset were downloaded from the Sequence Read Archive using fastq-dump from sratoolkit. This included datasets focusing on H3K27ac modifications in cortical neurons (GSM1629381, GSM1629397)(*37*) examining ACSS2 regulation of histone acetylation in hippocampal memory (GSM2415913, GSM2415912)(*35*) and investigating H3K18 crotonylation in macrophages (GSM1559471, GSM1559473, GSM1559472, GSM1559474) (*15*). We then ran the script ChIP-seq_SE_pipeline.sh for each raw dataset and normalized results by their respective ChIP-seq inputs

using the script subtractTwoWig.py. Peak calling was performed using MACS2, and identified peaks were overlapped with gene annotations within a region spanning 2,000 base pairs upstream to 1,000 base pairs downstream of the transcription start site (TSS). The resulting gene lists were then compared using Venn diagrams, and we further analyzed these lists by overlapping them with induced activity genes from a published nuRNA-seq study (*2*) to associate fold change values with different gene sets harboring distinct epigenetic marks.

Histone extraction: Histone extraction was performed using a commercially available kit (Histone Extraction Kit, Active Motif, #40028) according to the manufacturer's protocol. Briefly, flash frozen hippocampi were mechanically homogenized in 300 µl of ice-cold Lysis Buffer AM8 using Dounce homogenizers and incubated on ice for 30 mins. The homogenate was centrifuged at 2,644 x g for 2 minutes at 4°C, and the nuclear pellet was resuspended in 250 µl ice-cold Extraction buffer. Following resuspension, the nuclear suspension was incubated on an end-to-end rotator overnight at 4°C. The pellet insoluble material was centrifuged at 20,800 x g for 10 minutes at 4°C the next day, the supernatant was collected, and the requisite volume of Complete Neutralization Buffer was added. Samples were stored in -80^{o}C prior to western blotting.

Western blot analysis: Western blotting was performed as previously described (*4, 33*). Whole cell lysates were run on a 4–20% Tris-HCl Protein Gel (BIO-RAD, #3450033). Proteins from the gel were then transferred to methanol-activated polyvinylidene difluoride membranes using the Trans-Blot Turbo Transfer System (BIO-RAD). Membranes were blocked with the Odyssey® Blocking Buffer (LI-COR) diluted in TBS and incubated overnight at 4°C with the following primary antibodies: pan-Kcr (1:1000, PTM BIO, #PTM-501), Total H3 (1:5000, ACTIVE MOTIF, #61647), ACSS2 (1:1000, Cell Signaling, #3658), and Actin (1:10,000, #MA1-91399). Post primary antibody incubation, membranes were washed thrice in TBS for 5 mins and incubated with anti-rabbit IRDye 800LT (1:5,000, LI-COR, #926-32211) and anti-mouse IRDye 680CW (1:5000, LI-COR, #926-68022). Membranes were then washed thrice in TBS, 5 mins each. Images were acquired using the Odyssey Infrared Imaging System (LI-COR). Quantification of western blot bands was performed using Image Studio Lite ver5.2 (LI-COR).

***Immunofluorescence and confocal imaging*:** IHC experiments were performed as per earlier studies (*4, 33*). Animals were perfused with 4% PFA. Whole brains were harvested, immersed in 4% PFA, and stored at 4^{o}C. 24 hrs after, brains were immersed in 30% sucrose and stored at 4^{o}C. 20 µm coronal brain sections were made in a cryostat (Leica). Free-floating sections were washed thrice with PBS, blocked in a blocking buffer (0.1% PBST and 5% BSA) and incubated with the following primary antibodies for 48 hr: pan-Kcr (1:2000, PTM BIO, #PTM-501), CDYL (1:500, Sigma, #HPA035578), V5

(1:500, ThermoFisher Scientific, #37-7500), and GFP (1:4000, Abcam, #ab290). Post primary antibody incubation, sections were washed in PBS thrice, followed by a 2 hr secondary antibody incubation with the following antibodies: Goat anti-Mouse IgG (H+L) Cross-Adsorbed Secondary Antibody, Alexa Fluor™ 546 (1:500, ThermoFisher Scientific, #A-11003), Goat anti-Rabbit IgG (H+L) Cross-Adsorbed Secondary Antibody, Alexa Fluor™ 647 (1:500, ThermoFisher Scientific, #A-21244). Sections were then washed thrice in PBS and mounted on Superfrost™ Plus microscope slides (Fisherbrand). This was followed by coverslip mounting with ProLong™ Diamond Antifade Mountant with DAPI (ThermoFisher Scientific, #P36962).

In situ hybridization (RNAscope): *In situ* hybridization was performed using the RNAscope™ Multiplex Fluorescent Reagent Kit v2 (Advanced Cell Diagnostics) according to the manufacturer's protocol as previously described(*4*). Briefly, 20 µm cryosections obtained from fixed frozen brains were mounted on Superfrost™ Plus microscope slides (Fisherbrand). Slides then underwent serial dehydration in Ethanol, followed by Hydrogen Peroxide treatment, Target Retrieval, and Protease III treatment. Hybridization of probes was done at 40°C for 2 hr in an HybEZ oven using a probe against *Gria4.* The probe signal was amplified with Pre-amplifiers (AMP 1-FL, AMP 2-FL, and AMP 3-FL) and counterstained with OPAL 570 reagent (#FP1488001KT, Akoya Biosciences). Finally, coverslip mounting was done on the slides using ProLong™ Diamond Antifade Mountant with DAPI (ThermoFisher Scientific, P36962). The slides were stored in 4^0C until they were imaged.

***Adeno-associated virus (AAV) constructs and stereotactic surgeries*:** AAV_9-CaMKIIα-EGFP and AAV_9-CaMKIIα-CDYL-V5 were purchased from VectorBuilder (VectorBuilder Inc). AAV_9-CaMKIIα-GFP-Cre was purchased from Addgene (#105551). Mice were anesthetized using 5% isoflurane. A steady flow of 2.5% isoflurane was maintained throughout the remainder of the stereotactic surgery. 1 µl of respective AAVs were bilaterally injected into the dorsal hippocampus (coordinates: anteroposterior, −1.9 mm, mediolateral, ±1.5 mm, and 1.5 mm below bregma). Following viral infusion, drill holes were closed with bone wax (Lukens) and the incisions were sutured. Intraperitoneal (IP) injections of Meloxicam (5 mg/kg) were administered for 5 successive days after the surgery to manage the post-operative pain.

***Spatial object recognition (SOR) task*:** All the behavioral experiments were performed based on previously published studies(*4, 33*) during the light cycle in between Zeitgeber time (ZT) 0 through 2. Mice were individually housed for 7 days before the training. Animals were handled for 2 mins each day for 5 successive days before training. In the strong training paradigm, animals were habituated in an open field for 6 minutes. This was followed by three 6-minute sessions inside the same arena

containing three different glass objects. These objects were placed at specific spatial coordinates with respective to a spatial cue within the arena. An inter-trial interval of 5 minutes was set in-between the three training sessions. In the sub-threshold training paradigm, mice were subjected to three 3-minute training trials in the open field with two objects and an inter-trial interval of 5 minutes in between sessions. 24 hr after training, the animals were returned to the arena with one of the objects displaced to a novel spatial coordinate. Exploration time around all the objects were then manually scored. Percent preference towards the displaced object was calculated using the following equation:

$$\textit{Percent preference for displaced object} = \frac{(exploration\ towards\ the\ displaced\ object)}{(total\ exploration\ towards\ all\ objects)}\ x\ 100$$

For the histone Kcr profiling and the single nuclei experiments, animals were euthanized by cervical dislocation 1 hr after the last training trial in the SOR task. Hippocampal tissue was flash frozen and stored at -80^{0}C. Home caged animals were euthanized within the same ZT window to eliminate the possible confounding effects of circadian rhythmicity. To examine the learning-induced expression of Kcr in hippocampal subregions, mice were perfused 1 hr after the training session, and whole brains were harvested for IHC.

Contextual fear conditioning: Contextual fear conditioning was performed using a sub-threshold learning paradigm. In brief, mice were handled daily for five days before conditioning. The conditioning protocol involved a single 2-second, 0.75 mA footshock delivered 2.5 minutes after the mice were introduced into the chamber. Mice remained in the chamber for an additional 30 seconds before being returned to their home cage. Twenty-four hours later, they were reintroduced to the same chamber for 5 mins. Freezing behavior was assessed using FreezeScan software (CleverSys Inc.).

Nuclei isolation: Nuclei isolation form frozen hippocampal tissue was performed according to the manufacturer's protocol (Chromium Nuclei Isolation Kit with RNAse Inhibitor, 10x Genomics, #1000494). Briefly, frozen tissue was homogenized in 500 µl of Lysis Buffer using Dounce homogenizers. The lysate was transferred to a Nuclei Isolation Column and centrifuged at 16,000 rcf for 30 seconds at 4^{o}C. The pellet was then resuspended in 500 µl of Debris Removal Buffer and centrifuged at 700 rcf for 10 minutes at 4^{o}C. The nuclear pellet was then resuspended with 1 ml of Wash Buffer and centrifuged at 500 rcf for 5 minutes at 4^{o}C. Finally, the nuclear pellet was resuspended in 50 µl of Resuspension Buffer. Nuclei count was manually done using a Hemocytometer.

Single nuclei multiomic data processing and analysis: Raw sequencing data were processed using the 'Cell Ranger ARC' pipeline (v2.0.2) with the cell ranger-arc mm10 reference. Default parameters

were used to align reads, count unique fragments or transcripts, and filter high-quality nuclei. HDF5 files for each sample (Saline1, Saline2, Crotonate1, Crotonate2) containing barcoded RNA counts and ATAC fragments per cell cluster were loaded into Seurat (Read10X_h5). This resulted in the generation of four Seurat objects, each containing both RNA and ATAC assays. Nuclei with outliers within the ATAC and RNA QC metrics (<200 and >100,000 ATAC read counts, <200 and >50,000 RNA read counts, nucleosomal signal > 4, TSS enrichment < 3, %reads in peaks < 15 and percentage of mitochondrial reads > 5) were removed.

To analyze the RNA component of the multiomics data, gene counts were normalized, and log transformed (LogNormalize). The top 2,000 most variable features that distinguish each cell were identified using 'FindVariableFeatures' (selection.method = 'vst'). Features that are repeatedly variable across cells and datasets were selected for integration ('SelectIntegrationFeatures'). We then identified anchors ('FindIntegrationAnchors''), which took the list of 4 individual Seurat objects for each sample as input. These anchors were used to integrate the four datasets together ('IntegrateData'). Linear dimensionality reduction was performed on the integrated Seurat object by principal component analysis (runPCA, npcs = 30). A k-nearest-neighbours graph was constructed based on Euclidean distance in PCA space and refined ('FindNeighbors'), following which the nuclei were clustered using the Louvain algorithm (FindClusters, resolution = 0.5). Clusters were visualized with UMAP (runUMAP, dims = 30). Both RNA and ATAC assays were used to identify cell-type specific signatures of biomarkers. Differentially expressed genes (DEGs) in individual clusters between saline and crotonate treated groups were calculated (FindMarkers, test.use = 'wilcox,' Padj < 0.05, absolute logFC.threshold of 0.2).

To analyze the ATAC component of the multiomics data, the default assay was switched to ATAC prior to integrating the four Seurat objects, and peak calling was performed. The set of peaks identified by 'Cellranger' often merges distinct peaks that are close together - confounding the motif enrichment analysis and peak-to-gene linkage. We were able to circumvent this concern and identify a more accurate set of peaks by using the 'MACS2' (CallPeaks) peak calling feature on all cells together. Peaks on nonstandard chromosomes and in genomic blacklist regions were removed ('keepStandardChromosomes' and 'subsetByOverlaps'). A frequency-inverse document frequency normalization was performed across cells and peaks ('RunTFIDF'). Thereafter, a feature selection was performed using all the peaks as input (FindTopFeatures, min.cutoff = 5). The selected peaks went through a dimensional reduction on the TF-IDF normalized matrix using a singular value decomposition ('RunSVD'). To identify the differentially accessible regions (DAR) between crotonate versus saline group, the Seurat function 'FindMarkers' was used using logistic regression (LR) as a method to test

significance. The DARs with adjusted p value < 0.05 and absolute log2foldchange threshold of above 0.2 were considered as significantly differentially accessible. Further, the DARs were annotated using 'Closestfeature' function from Signac package as well as 'annotatePeak' function from 'ChIPseeker' package. The DEGs were furthered correlated with DARs where the DARs were selected only from the promoter (+/- 2kb from transcription start site) and genebody regions, filtering out the peaks from distal genomic regions and downstream of 3'UTR(*74*). The genes found concordant in both DEG and DAR lists were shortlisted for downstream gene ontology enrichment analysis. UpSet plots were generated using UpSetR package.

Gene Ontology enrichment analysis: The concordant DARs and DEGs were analyzed for Molecular Function (MF) enrichment analysis by using the 'clusterProfiler' package with the default criteria (pvalueCutoff = 0.01 and qvalueCutoff = 0.05). Here, the significant upregulated DEGs (adj p value < 0.05 and log2FC > 0.2) concordant with the significant more accessible DARs (adj p value < 0.05 and log2FC > 0.2) were used to generate the upregulated gene list, whereas the significant downregulated DEGs (adj p value < 0.05 and log2FC < -0.2) concordant with the significant less accessible DARs (adj p value < 0.05 and log2FC < -0.2) were used to generate the downregulated gene list. The DARs were selected only from the promoter (+/- 2kb from transcription start site) and genebody regions filtering out the peaks from distal genomic regions and downstream of 3'UTR. All further data visualizations were made using clusterProfiler package.

TF motif enrichment analysis: To identify cell-type specific regulatory sequences, we performed transcription factor motif enrichment analysis on the DEGs that were found to have concordant differentially accessible peaks in the promoter region. Here, we restricted TF motif enrichment only in the promoter region (a window of 2000bp upstream and downstream of transcription start site). Motif enrichment was performed using 'FindMotifs' function of signac package. The motifs that had adjusted p value < 0.05 were considered significant. The top 15 significant motifs from the clusters were plotted as heatmap using ComplexHeatmap package. Weight matrices for the top motifs were also plotted to visualize the motif sequences.

Cell-cell communication analysis: The cell-cell communication analysis on the snRNA-seq data was performed using CellChat (v2.1.2). The Saline and Crotonate RNA normalized counts were taken and individual cellchat objects were created. Ligand-receptor (LR) interactions in each group were calculated by identifying overexpressed ligands or receptors with a log fold change cutoff 0.1 (identifyOverExpressedGenes(thresh.fc = 0.1, thresh.p = 0.05)) followed by identifying interactions if LR pairs are overexpressed (identifyOverExpressedInteractions). To assign each interaction with a

probability score, computeCommunProb function was used with a default statistical method called 'trimean'. Cell-cell communication was filtered to have minimum cell number 10 in each cell group (filterCommunication(min.cells = 10)). After that communication probability on signaling pathway level was calculated by summarizing the communication probabilities of all LR interactions associated with each signaling pathway. Finally, the cell-cell communication network was aggregated by counting the number of links or summarizing the communication probability amongst the cell groups. Thereafter, the cellchat objects were merged and compared using netVisual_aggregate, netAnalysis_signalingChanges_scatter, and netVisual_chord_gene functions.

Confocal imaging and image analysis: Confocal images of IHC experiments were obtained in an Olympus FV 3000 confocal microscope using a 20X NA = 0.4 achromat dry objective at 800 × 800-pixel resolution and 1X optical zoom. All images (16 bit) were acquired with identical settings for laser power, detector gain and pinhole diameter for each experiment and between experiments. Images from the different channels were stacked and projected at maximum intensity using ImageJ (NIH). Mean Fluorescence Intensity (MFI) was computed using ImageJ plugins.

Statistics: Behavioral and biochemical data were analyzed using unpaired two-tailed t-tests, one-way ANOVA, or two-way ANOVAs (sometimes with repeated measures as the within-subject variable). Sidak's multiple comparison tests or Dunnett's multiple comparison tests were used for post-hoc analyses wherever required. Differences were considered statistically significant when $p<0.05$. As indicated for each figure panel, all data were plotted in box plots.

Ethics: All procedures on mice in this study were conducted according to US National Institutes of Health guidelines for animal care and use and were approved by the Institutional Animal Care and Use Committee of the University of Iowa, Iowa.

Reporting summary: Further information on research design is available in the Nature Portfolio Reporting Summary linked to this article.

Figure 1. Histone Kcr levels are induced after spatial learning in the dorsal hippocampus. **a.** Venn diagram depicting the enrichments of ACSS2, H3k18cr, and H3k27ac on gene promoters (-2000bp to +500bp from TSS) obtained from ChIP-Seq datasets (*15, 35, 37*). **b.** Box plots showing the extent of gene induction in the hippocampus following neuronal stimulation in the hippocampus(*2*) for genes that exhibit ACSS2 and H3k27ac binding in the promoter region compared to genes that exhibit binding of ACSS2, H3k27ac, and H3k18cr in the promoter region. **c.** Schematic of the experiments performed in **d-i** to examine changes in KCr after learning. **d., e.** Western blot showing histone crotonylation analyzed from the dorsal hippocampus of mice trained in spatial object recognition (SOR)

task and euthanized at 0.5, 1, or 2h after training. Homecage (HC) mice were used as controls. One-way ANOVA: Kcr: $F_{(3, 27)}$=3.953, p= 0.0185. Dunnett multiple comparisons tests: *p=0.0379 (HC versus 1 hr). Homecage (n□=□8), SOR + 0.5 hr (n□=□7), SOR + 1 hr (n=8), SOR + 2 hr (n=8), males only. **f., i.** Immunofluorescence using anti-Kcr antibody showing levels of Kcr in different hippocampal sub-regions of HC and learning (SOR+1hr) mice. Normalized Mean Fluorescent Intensity (MFI) of nuclear Kcr levels across the groups. For CA1: unpaired t test: t (6)□= 3.810, **p□=□0.0089. Homecage (n□=□4) and SOR+1 hr (n□=□4), males only. For CA3: unpaired t test: t (6) = 0.2749, p□=□0.7926. Homecage (n□=□4) and SOR+1 hr (n□=□4), males only. For DG upper blade (U): unpaired t test: t (6)□= 3.118, *p□=□0.0206. Homecage (n□=□4) and SOR+1 hr (n□=□4), males only. For DG lower blade (L): unpaired t test: t (6)□= 0.5452, p□=□0.605. Homecage (n□=□4) and SOR+1 hr (n□=□4), males only. For subiculum: unpaired t test: t (6)□= 2.733, *p□=□0.034. Homecage (n□=□4) and SOR+1 hr (n□=□4), males only. All box plots: the center line represents the median, the box edges represent the top and bottom quartiles (25th to 75th percentiles), and the minimum and maximum whiskers.

Figure 2. Overexpression of Chromodomain Y-like protein (CDYL) in the dorsal hippocampus of mice impairs long-term spatial memory. **a.** Depiction of enzymes linked to histone crotonylation. **b.** Schematic of the experiments performed in **c-f**. **c-f.** Immunofluorescence using an anti-CDYL antibody was performed on brain slices from mice 1 hr after training in the SOR task. Hippocampal sub-regions CA1, CA3, DG upper blade (U), DG lower blade (L), and subiculum were studied. Normalized Mean Fluorescent Intensity (MFI) of nuclear CDYL levels across the groups. For CA1: Unpaired t test: t (6)□= 3.598, *p□=□0.0114. Homecage (n□=□4) and SOR+1 hr (n□=□4), males only. For CA3: Unpaired t test: t (6) = 1.704, p□=□0.1393. Homecage (n□=□4) and SOR+1 hr (n□=□4), males only. For DG upper blade: Unpaired t test: t (6)□= 3.254, *p□=□0.0174. Homecage (n□=□4) and SOR+1 hr (n□=□4), males only. For DG lower blade: Unpaired t test: t (6)□= 0.7837, p□=□0.463. Homecage (n□=□4) and SOR+1 hr (n□=□4), males only. For Subiculum: Unpaired t test: t (6)□= 3.657, *p□=□0.0106. Homecage (n□=□4) and SOR+1 hr (n□=□4), males only. **g.** Schematic of viral constructs infused in the dorsal hippocampus of adult male mice. AAV_9-CaMKIIα-EGFP served as vector control and AAV_9-CaMKIIα-CDYL-V5 was used to drive expression of CDYL in excitatory neurons. **h.** Immunofluorescence image using V5 antibody showed expression of CDYL-V5 in dorsal hippocampus after two weeks following viral infusion. **i-j.** Immunofluorescence image of the dorsal hippocampus using pan-Kcr antibody 1 hr after SOR training in CDYL-V5 or vector control expressing mice. Normalized Mean Fluorescent Intensity (MFI) of nuclear Kcr levels across the groups. For CA1: Unpaired t test: t (5)□= 2.679, *p□=□0.439. EGFP (n□=□3) and CDYL (n□=□4), males only. For CA3: Unpaired t test: t (5) = 3.417, *p□=□0.0189. EGFP (n□=□3) and CDYL (n□=□4), males only. For DG:

669 Unpaired t test: t (5)□= 1.863, p□=□0.1215. EGFP (n□=□3) and CDYL (n□=□4), males only. **k-l**.
670 Long-term memory (24 hr) assessment of mice infused with AAV-EGFP or AAV-CDYL into dorsal
671 hippocampus. Two-way ANOVA: significant session x virus interaction $F_{(1,13)}$=6.323, p=0.0259, Sidak's
672 multiple comparison tests, **p=0.0041 (EGFP 24 hr Test vs CDYL 24 hr Test) and **p=0.0051 (EGFP
673 Training vs EGFP 24 hr Test); AAV-EGFP (n=7), AAV-CDYL (n=8), males only. All box plots: the center
674 line represents the median, the box edges represent the top and bottom quartiles (25th to 75th
675 percentiles), and the minimum and maximum whiskers.

676 **Figure 3.** ***Increasing Kcr levels in the dorsal hippocampus enhances long-term memory.*** **a-b.** Kcr
677 Western blots of core histones extracted from dorsal hippocampus 1 hr after crotonate treatment (50
678 mg/kg or 200 mg/kg dose). Vehicle (saline) treated mice were used as controls. One-way ANOVA: Kcr:
679 $F_{(2, 14)}$ = 5.550, p=0.0168. Dunnett's multiple comparisons tests: *p= 0.0108 (saline versus crotonate
680 200mg/kg). Saline (n=6), Crotonate 50 mg/kg (n=6), Crotonate 200 mg/kg (n=5), males only. **c.** Long-
681 term memory enhancement in a sub-threshold SOR learning paradigm following crotonate treatment.
682 Two-way ANOVA: significant session x treatment interaction $F_{(2, 23)}$ = 5.081, p= 0.0149, Sidak's post
683 hoc tests, *p=0.0359 (200mg/kg crotonate 24 hr test vs saline 24 hr test), **p=0.0021 (200mg/kg
684 crotonate train vs 200mg/kg crotonate 24 hr test), **p=0.0025 (200mg/kg crotonate 24 hr test vs
685 50mg/kg crotonate 24 hr test). Saline (n=9), Crotonate 50 mg/kg (n=7), Crotonate 200 mg/kg (n=10),
686 males only. **d.** Long-term memory in a sub-threshold CFC learning paradigm following crotonate
687 treatment. Two-way ANOVA: Significant session x treatment interaction $F_{(2, 19)}$ = 4.946, *p=0.0187,
688 main effect of session (pre-shock and 24hr test): $F_{(1, 19)}$ = 140.9, p<0.0001. Sidak's post hoc tests,
689 *p=0.0130 (200mg/kg crotonate 24 hr test vs 50mg/kg crotonate 24 hr test), **p=0.0051 (200mg/kg
690 crotonate 24 hr test vs saline 24hr test). ****p<0.0001 (Saline pre-shock vs saline 24hr test),
691 ****p<0.0001 (crotonate 50mg/kg pre-shock vs crotonate 50mg/kg 24hr test), and ****p<0.0001
692 (crotonate 200mg/kg pre-shock vs crotonate 200mg/kg 24hr test). Saline (n=8), Crotonate 50 mg/kg
693 (n=6), Crotonate 200 mg/kg (n=8), males only. All box plots: the center line represents the median, the
694 box edges represent the top and bottom quartiles (25th to 75th percentiles), and the minimum and
695 maximum whiskers.

696 ***Figure 4. Crotonate-mediated memory enhancement is dependent on ACSS2.*** **a.** Schematics of
697 ACSS2 in regulating histone crotonylation. **b.** Schematic of viral constructs used to conditionally knock
698 down ACSS2 in excitatory neurons of dorsal hippocampus. AAV_9-CaMKIIα-EGFP served as vector
699 control and AAV_9-CaMKIIα-Cre-EGFP was used to drive expression of Cre recombinase in excitatory
700 neurons of $ACSS2^{f/f}$ mice. **c.** Immunofluorescence image using GFP antibody showed expression of
701 the Cre-EGFP in the dorsal hippocampus two weeks following viral infusion. **d-e.** Western blot from

whole cell extracts of the dorsal hippocampus of ACSS2$^{f/f}$ mice infused with AAV-EGFP or AAV-Cre-EGFP. Normalized band intensity of ACSS2 across the groups: Unpaired t test: t (4)□= 4.118, *p□=□0.0146. EGFP (n□=□3) and ACSS2 (n□=□3), males only. **f-g.** Western blot using Kcr antibody from core histones extracted from the dorsal hippocampus of ACSS2 cKO mice (ACSS2$^{f/f}$ infused with AAV-Cre-EGFP) administered either crotonate (200 mg/kg, oral gavage) or saline immediately after SOR training. Normalized band intensity of pan Kcr across the groups: Unpaired t test: t (4)□= 0.1853, p□=□0.862. Saline (n=3), Crotonate (n=3), males only. **h-i.** Crotonate treatment after training using a sub-threshold SOR learning paradigm does not enhance long-term memory in ACSS2 cKO mice. Two-way ANOVA: no significant session x treatment interaction $F_{(1, 10)}$ = 0.0007554, p= 0.9786. Saline (n=6), Crotonate (n=6), males only. All box plots: the center line represents the median, the box edges represent the top and bottom quartiles (25th to 75th percentiles), and the minimum and maximum whiskers.

Figure 5. ***Single-nuclei multiomics (RNA+ATAC-seq) reveals cell type-specific gene expression and chromatin accessibility changes mediated by crotonate*****. a.** Experimental scheme. Adult male C57BL/6J mice were trained in a sub-threshold SOR paradigm and administered with crotonate (200 mg/kg, oral gavage; n=4) or saline (oral gavage; n=4) immediately after the completion of training. One hour later, the dorsal hippocampus was harvested, and nuclei were isolated for single nuclei multiomics processing. Hippocampi from two animals within the same group were pooled for each droplet capture, resulting in a final sample size of n=2 per group for the single nuclei multiomics analysis. **b.** UMAP plot showing cell type-specific clusters of the dorsal hippocampus. **c.** Violin plot showing the expression profiles of marker genes across different cell types of the dorsal hippocampus. **d.** Volcano plots depicting genes that exhibit differential expression and chromatin accessibility following crotonate treatment. Genes labeled with color are DEGs that also exhibit DARs. **e-h.** Cnet plot shows the top five enriched pathways (GO: Molecular Function) and their respective differentially accessible DEGs in hippocampal subregions CA1 **(e)**, CA3 **(f)**, Subiculum **(g)**, and Dentate gyrus **(h)**.

Figure 6. ***Cell-cell communication analyses reveal crotonate-mediated alterations in the strength and nature of communicative pathways within the hippocampal circuit. a.*** Differential incoming interaction strength and differential outgoing interaction strength in crotonate-treated mice compared to saline-treated mice in hippocampal subregions CA1, CA3, Subiculum, and DG. **b.** Individual ligand-receptor interactions significantly enhanced upon crotonate treatment in intrahippocampal projections of DG-CA3, CA3-CA1, and CA1-subiculum. **c.** Interaction strength of ligand-receptor genes involved in glutamatergic signaling across the principal hippocampal neuronal networks in saline-treated and crotonate-treated mice. Communication probability, represented by numbers ranging from 0 to 10, is

visualized through the edge width of intrahippocampal connections, indicating the strength of communication between the respective subregions. **d.** Violin plot depicting expression of *Gria4* mRNA in hippocampal principal neuronal cell types across saline- and crotonate-treated conditions. **e-h.** RNAscope of *Gria4* in hippocampal CA1 (**e-f**) and subiculum (**g-h**) sub-regions. Mice were trained with a sub-optimal SOR training protocol, administered saline or crotonate (200 mg/kg) immediately after training, and perfused 1 hr later. **f.** Quantification of *Gria* in CA1. Normalized Mean Fluorescent Intensity (MFI) of Gria4 levels across the groups. Unpaired t test: t (6)□= 2.613, *p□=□0.04. Homecage (n□=□4) and SOR+1 hr (n□=□4), males only. **h.** Quantification of *Gria* in subiculum. Normalized Mean Fluorescent Intensity (MFI) of *Gria4* levels across the groups. Unpaired t test: t (6)□= 3.019, *p□=□0.0234. Homecage (n□=□4) and SOR+1 hr (n□=□4), males only. Box plots: the center line represents the median, the box edges represent the top and bottom quartiles (25th to 75th percentiles), and the minimum and maximum whiskers.

Acknowledgments

We thank the Neural Circuits and Behavior Core and the Iowa Institute of Human Genetics (IIHG) core for using their facilities, Emily N. Walsh, Quinlan Truax, Adam J Rauckhorst, and Rebekah M. Peplinski for their technical assistance, and K. Peter Giese and Jacob Michaelson for their valuable input on this work.

Funding

This work was supported by grants from the National Institute of Health R01 MH 087463 to T.A., Alzheimer's Association Research Grant AARG-23-1074289 to SC, and The National Institute of Health R00 AG068306 to S.C. T.A. is also supported by the Roy J. Carver Charitable Trust. The sequencing data presented herein were obtained at the Genomics Division of the Iowa Institute of Human Genetics (RRID: SCR_023422), which is supported, in part, by the University of Iowa Carver College of Medicine.

Author contributions

S.C. and T.A. conceived the study. S.C. and U.M. designed the experiments, interpreted the results, and wrote the article with inputs from T.A. and E.B.T. U.M., S.C., and S.E.B. performed the behavioral tasks, stereotactic surgeries, drug treatment, and biochemical experiments. S.G. and N.R. assisted with the analysis of behavioral data and biochemical experiments. E.B.T. provided the ACSS2 mice. B.B. performed the bioinformatic analyses with inputs from Y.V.

Declaration of interests

T.A. serves on the Scientific Advisory Board of EmbarkNeuro and is a scientific advisor to Aditum Bio and Radius Health. The other authors declare no conflicting interests.

Data availability

The datasets generated in this study have been deposited in the NCBI Gene Expression Omnibus (GEO) database under accession code GSE281007. Sequencing files for the single nuclei multiomics (RNA-seq + ATAC-seq) have been made publicly available through GSE281007.

Code availability

The code used for the analyses to generate the figures related to Single nuclei multiomics data can be accessed through GitHub (https://github.com/ChatterjeeEpigenetics/CrotonylationMultiomics2024).

References

1. E. L. Yap, M. E. Greenberg, Activity-Regulated Transcription: Bridging the Gap between Neural Activity and Behavior. *Neuron* **100**, 330-348 (2018).
2. J. Fernandez-Albert *et al.*, Immediate and deferred epigenomic signatures of in vivo neuronal activation in mouse hippocampus. *Nat Neurosci* **22**, 1718-1730 (2019).
3. K. M. Tyssowski *et al.*, Different Neuronal Activity Patterns Induce Different Gene Expression Programs. *Neuron* **98**, 530-546 e511 (2018).
4. Y. Vanrobaeys *et al.*, Mapping the spatial transcriptomic signature of the hippocampus during memory consolidation. *Nat Commun* **14**, 6100 (2023).
5. J. Graff, B. T. Woldemichael, D. Berchtold, G. Dewarrat, I. M. Mansuy, Dynamic histone marks in the hippocampus and cortex facilitate memory consolidation. *Nat Commun* **3**, 991 (2012).
6. J. M. Levenson *et al.*, Regulation of histone acetylation during memory formation in the hippocampus. *J Biol Chem* **279**, 40545-40559 (2004).
7. I. Maze, K. M. Noh, C. D. Allis, Histone regulation in the CNS: basic principles of epigenetic plasticity. *Neuropsychopharmacology* **38**, 3-22 (2013).
8. L. Peixoto, T. Abel, The role of histone acetylation in memory formation and cognitive impairments. *Neuropsychopharmacology* **38**, 62-76 (2013).
9. I. B. Zovkic, M. C. Guzman-Karlsson, J. D. Sweatt, Epigenetic regulation of memory formation and maintenance. *Learn Mem* **20**, 61-74 (2013).
10. B. R. Sabari, D. Zhang, C. D. Allis, Y. Zhao, Metabolic regulation of gene expression through histone acylations. *Nat Rev Mol Cell Biol* **18**, 90-101 (2017).
11. E. Verdin, M. Ott, 50 years of protein acetylation: from gene regulation to epigenetics, metabolism and beyond. *Nat Rev Mol Cell Biol* **16**, 258-264 (2015).
12. C. E. Barnes, D. M. English, S. M. Cowley, Acetylation & Co: an expanding repertoire of histone acylations regulates chromatin and transcription. *Essays Biochem* **63**, 97-107 (2019).
13. O. Bousiges *et al.*, Spatial memory consolidation is associated with induction of several lysine-acetyltransferase (histone acetyltransferase) expression levels and H2B/H4 acetylation-

dependent transcriptional events in the rat hippocampus. *Neuropsychopharmacology* **35**, 2521-2537 (2010).

14. S. Peleg *et al.*, Altered histone acetylation is associated with age-dependent memory impairment in mice. *Science* **328**, 753-756 (2010).

15. B. R. Sabari *et al.*, Intracellular crotonyl-CoA stimulates transcription through p300-catalyzed histone crotonylation. *Mol Cell* **58**, 203-215 (2015).

16. Z. Kaczmarska *et al.*, Structure of p300 in complex with acyl-CoA variants. *Nat Chem Biol* **13**, 21-29 (2017).

17. T. Abel, K. C. Martin, D. Bartsch, E. R. Kandel, Memory suppressor genes: inhibitory constraints on the storage of long-term memory. *Science* **279**, 338-341 (1998).

18. S. Bahari-Javan *et al.*, HDAC1 regulates fear extinction in mice. *J Neurosci* **32**, 5062-5073 (2012).

19. J. S. Guan *et al.*, HDAC2 negatively regulates memory formation and synaptic plasticity. *Nature* **459**, 55-60 (2009).

20. J. M. Alarcon *et al.*, Chromatin acetylation, memory, and LTP are impaired in CBP+/- mice: a model for the cognitive deficit in Rubinstein-Taybi syndrome and its amelioration. *Neuron* **42**, 947-959 (2004).

21. E. Korzus, M. G. Rosenfeld, M. Mayford, CBP histone acetyltransferase activity is a critical component of memory consolidation. *Neuron* **42**, 961-972 (2004).

22. M. Tan *et al.*, Identification of 67 histone marks and histone lysine crotonylation as a new type of histone modification. *Cell* **146**, 1016-1028 (2011).

23. E. R. Abu-Zhayia, F. E. Machour, N. Ayoub, HDAC-dependent decrease in histone crotonylation during DNA damage. *J Mol Cell Biol* **11**, 804-806 (2019).

24. M. Crespo *et al.*, Multi-omic analysis of gametogenesis reveals a novel signature at the promoters and distal enhancers of active genes. *Nucleic Acids Res* **48**, 4115-4138 (2020).

25. S. K. Dai *et al.*, Histone crotonylation regulates neural stem cell fate decisions by activating bivalent promoters. *EMBO Rep* **22**, e52023 (2021).

26. S. Liu *et al.*, Chromodomain Protein CDYL Acts as a Crotonyl-CoA Hydratase to Regulate Histone Crotonylation and Spermatogenesis. *Mol Cell* **67**, 853-866 e855 (2017).

27. O. Ruiz-Andres *et al.*, Histone lysine crotonylation during acute kidney injury in mice. *Dis Model Mech* **9**, 633-645 (2016).

28. Y. Zou *et al.*, Involvement of Histone Lysine Crotonylation in the Regulation of Nerve-Injury-Induced Neuropathic Pain. *Front Immunol* **13**, 885685 (2022).

29. Y. Li *et al.*, Molecular Coupling of Histone Crotonylation and Active Transcription by AF9 YEATS Domain. *Mol Cell* **62**, 181-193 (2016).

30. D. Zhao *et al.*, YEATS2 is a selective histone crotonylation reader. *Cell Res* **26**, 629-632 (2016).

31. A. Marco *et al.*, Mapping the epigenomic and transcriptomic interplay during memory formation and recall in the hippocampal engram ensemble. *Nat Neurosci* **23**, 1606-1617 (2020).

32. C. M. Alberini, E. R. Kandel, The regulation of transcription in memory consolidation. *Cold Spring Harb Perspect Biol* **7**, a021741 (2014).

33. S. Chatterjee *et al.*, Endoplasmic reticulum chaperone genes encode effectors of long-term memory. *Sci Adv* **8**, eabm6063 (2022).

34. L. Li *et al.*, Inhibition of ACSS2-mediated histone crotonylation alleviates kidney fibrosis via IL-1beta-dependent macrophage activation and tubular cell senescence. *Nat Commun* **15**, 3200 (2024).

35. P. Mews *et al.*, Acetyl-CoA synthetase regulates histone acetylation and hippocampal memory. *Nature* **546**, 381-386 (2017).

36. D. C. Alexander *et al.*, Targeting acetyl-CoA metabolism attenuates the formation of fear memories through reduced activity-dependent histone acetylation. *Proc Natl Acad Sci U S A* **119**, e2114758119 (2022).

37. F. Telese *et al.*, LRP8-Reelin-Regulated Neuronal Enhancer Signature Underlying Learning and Memory Formation. *Neuron* **86**, 696-710 (2015).

38. Y. Liu *et al.*, CDYL suppresses epileptogenesis in mice through repression of axonal Nav1.6 sodium channel expression. *Nat Commun* **8**, 355 (2017).

39. S. Chatterjee *et al.*, Pharmacological activation of Nr4a rescues age-associated memory decline. *Neurobiol Aging* **85**, 140-144 (2020).

40. A. J. Rauckhorst *et al.*, A hierarchical hepatic de novo lipogenesis substrate supply network utilizing pyruvate, acetate, and ketones. *Cell Metab*, (2024).

41. J. Basu, S. A. Siegelbaum, The Corticohippocampal Circuit, Synaptic Plasticity, and Memory. *Cold Spring Harb Perspect Biol* **7**, (2015).

42. J. Basu *et al.*, A cortico-hippocampal learning rule shapes inhibitory microcircuit activity to enhance hippocampal information flow. *Neuron* **79**, 1208-1221 (2013).

43. T. Klausberger, P. Somogyi, Neuronal diversity and temporal dynamics: the unity of hippocampal circuit operations. *Science* **321**, 53-57 (2008).

44. S. Jin *et al.*, Inference and analysis of cell-cell communication using CellChat. *Nat Commun* **12**, 1088 (2021).

45. Z. Guan *et al.*, Integration of long-term-memory-related synaptic plasticity involves bidirectional regulation of gene expression and chromatin structure. *Cell* **111**, 483-493 (2002).

46. X. Xiong *et al.*, Selective recognition of histone crotonylation by double PHD fingers of MOZ and DPF2. *Nat Chem Biol* **12**, 1111-1118 (2016).

47. S. J. Martin, P. D. Grimwood, R. G. Morris, Synaptic plasticity and memory: an evaluation of the hypothesis. *Annu Rev Neurosci* **23**, 649-711 (2000).

48. G. Neves, S. F. Cooke, T. V. Bliss, Synaptic plasticity, memory and the hippocampus: a neural network approach to causality. *Nat Rev Neurosci* **9**, 65-75 (2008).

49. M. B. Kennedy, Synaptic Signaling in Learning and Memory. *Cold Spring Harb Perspect Biol* **8**, a016824 (2013).

50. C. Mulle *et al.*, Altered synaptic physiology and reduced susceptibility to kainate-induced seizures in GluR6-deficient mice. *Nature* **392**, 601-605 (1998).

51. A. Contractor, G. Swanson, S. F. Heinemann, Kainate receptors are involved in short- and long-term plasticity at mossy fiber synapses in the hippocampus. *Neuron* **29**, 209-216 (2001).

52. C. Spanaki *et al.*, Glutamate-specific gene linked to human brain evolution enhances synaptic plasticity and cognitive processes. *iScience* **27**, 108821 (2024).

884 53. M. R. Taylor *et al.*, Kirrel3-Mediated Synapse Formation Is Attenuated by Disease-Associated
885 Missense Variants. *J Neurosci* **40**, 5376-5388 (2020).

886 54. E. A. Martin *et al.*, The intellectual disability gene Kirrel3 regulates target-specific mossy fiber
887 synapse development in the hippocampus. *Elife* **4**, e09395 (2015).

888 55. M. T. Haile, S. Khoja, G. de Carvalho, R. F. Hunt, L. Y. Chen, Conditional deletion of Neurexin-2
889 alters neuronal network activity in hippocampal circuitries and leads to spontaneous seizures.
890 *Transl Psychiatry* **13**, 97 (2023).

891 56. A. J. Wilk, A. K. Shalek, S. Holmes, C. A. Blish, Comparative analysis of cell-cell communication
892 at single-cell resolution. *Nat Biotechnol* **42**, 470-483 (2024).

893 57. S. Magi, S. Piccirillo, S. Amoroso, V. Lariccia, Excitatory Amino Acid Transporters (EAATs):
894 Glutamate Transport and Beyond. *Int J Mol Sci* **20**, (2019).

895 58. Y. Zhou, N. C. Danbolt, Glutamate as a neurotransmitter in the healthy brain. *J Neural Transm*
896 *(Vienna)* **121**, 799-817 (2014).

897 59. J. D. Pita-Almenar, M. S. Collado, C. M. Colbert, A. Eskin, Different mechanisms exist for the
898 plasticity of glutamate reuptake during early long-term potentiation (LTP) and late LTP. *J*
899 *Neurosci* **26**, 10461-10471 (2006).

900 60. J. Goncalves-Ribeiro, C. C. Pina, A. M. Sebastiao, S. H. Vaz, Glutamate Transporters in
901 Hippocampal LTD/LTP: Not Just Prevention of Excitotoxicity. *Front Cell Neurosci* **13**, 357
902 (2019).

903 61. S. M. Wojcik *et al.*, An essential role for vesicular glutamate transporter 1 (VGLUT1) in postnatal
904 development and control of quantal size. *Proc Natl Acad Sci U S A* **101**, 7158-7163 (2004).

905 62. D. S. Bredt, R. A. Nicoll, AMPA receptor trafficking at excitatory synapses. *Neuron* **40**, 361-379
906 (2003).

907 63. J. V. Negrete-Diaz, R. Falcon-Moya, A. Rodriguez-Moreno, Kainate receptors: from synaptic
908 activity to disease. *FEBS J* **289**, 5074-5088 (2022).

909 64. J. D. Nair *et al.*, Sustained postsynaptic kainate receptor activation downregulates AMPA
910 receptor surface expression and induces hippocampal LTD. *iScience* **24**, 103029 (2021).

911 65. M. M. Petrovic *et al.*, Metabotropic action of postsynaptic kainate receptors triggers
912 hippocampal long-term potentiation. *Nat Neurosci* **20**, 529-539 (2017).

913 66. J. F. Guzowski, B. L. McNaughton, C. A. Barnes, P. F. Worley, Environment-specific expression
914 of the immediate-early gene Arc in hippocampal neuronal ensembles. *Nat Neurosci* **2**, 1120-
915 1124 (1999).

916 67. S. A. Josselyn, S. Tonegawa, Memory engrams: Recalling the past and imagining the future.
917 *Science* **367**, (2020).

918 68. M. A. Wood, J. D. Hawk, T. Abel, Combinatorial chromatin modifications and memory storage: a
919 code for memory? *Learn Mem* **13**, 241-244 (2006).

920 69. B. D. Strahl, C. D. Allis, The language of covalent histone modifications. *Nature* **403**, 41-45
921 (2000).

922 70. G. Santoni *et al.*, Chromatin plasticity predetermines neuronal eligibility for memory trace
923 formation. *Science* **385**, eadg9982 (2024).

71. A. M. Burns *et al.*, The HDAC inhibitor CI-994 acts as a molecular memory aid by facilitating synaptic and intracellular communication after learning. *Proc Natl Acad Sci U S A* **119**, e2116797119 (2022).

72. Z. Wang *et al.*, NEAT1 regulates neuroglial cell mediating Abeta clearance via the epigenetic regulation of endocytosis-related genes expression. *Cell Mol Life Sci* **76**, 3005-3018 (2019).

73. Y. Liu *et al.*, Chromodomain Y-like Protein-Mediated Histone Crotonylation Regulates Stress-Induced Depressive Behaviors. *Biol Psychiatry* **85**, 635-649 (2019).

74. T. Stuart, A. Srivastava, S. Madad, C. A. Lareau, R. Satija, Single-cell chromatin state analysis with Signac. *Nat Methods* **18**, 1333-1341 (2021).

Figure 1

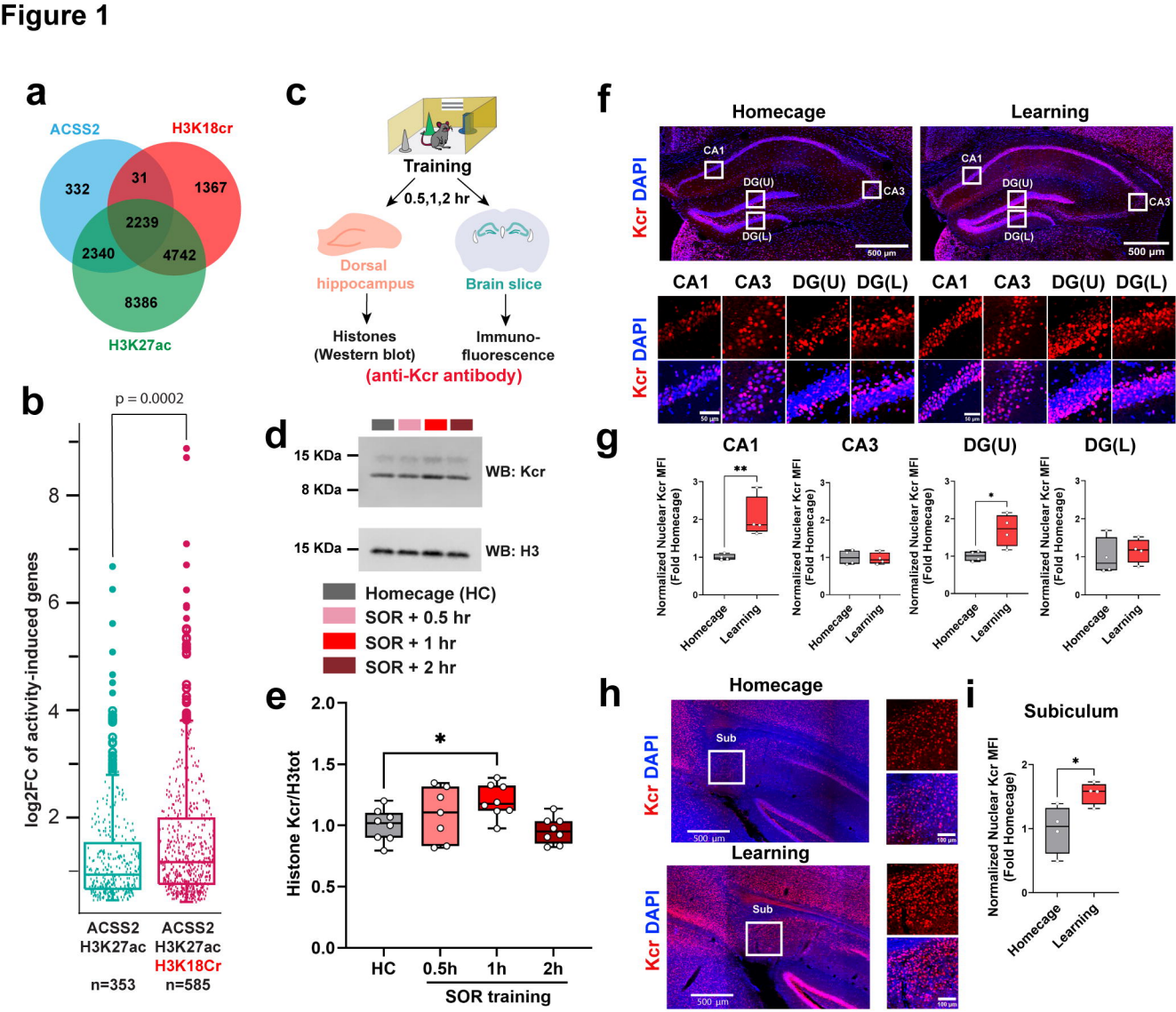
a
ACSS2
H3K18cr
H3K27ac
332
31
1367
2239
2340
4742
8386
b
p = 0.0002
log2FC of activity-induced genes
ACSS2 H3K27ac
ACSS2 H3K27ac H3K18Cr
n=353
n=585
c
Training
0.5,1,2 hr
Dorsal hippocampus
Brain slice
Histones (Western blot)
Immuno-fluorescence
(anti-Kcr antibody)
d
15 KDa
8 KDa
WB: Kcr
15 KDa
WB: H3
Homecage (HC)
SOR + 0.5 hr
SOR + 1 hr
SOR + 2 hr
e
Histone Kcr/H3tot
HC
0.5h
1h
2h
SOR training
f
Homecage
Learning
CA1
CA3
DG(U)
DG(L)
Kcr DAPI
500 μm
50 μm
g
CA1
CA3
DG(U)
DG(L)
Normalized Nuclear Kcr MFI (Fold Homecage)
Homecage
Learning
h
Homecage
Learning
Sub
Kcr DAPI
500 μm
100 μm
i
Subiculum
Normalized Nuclear Kcr MFI (Fold Homecage)
Homecage
Learning

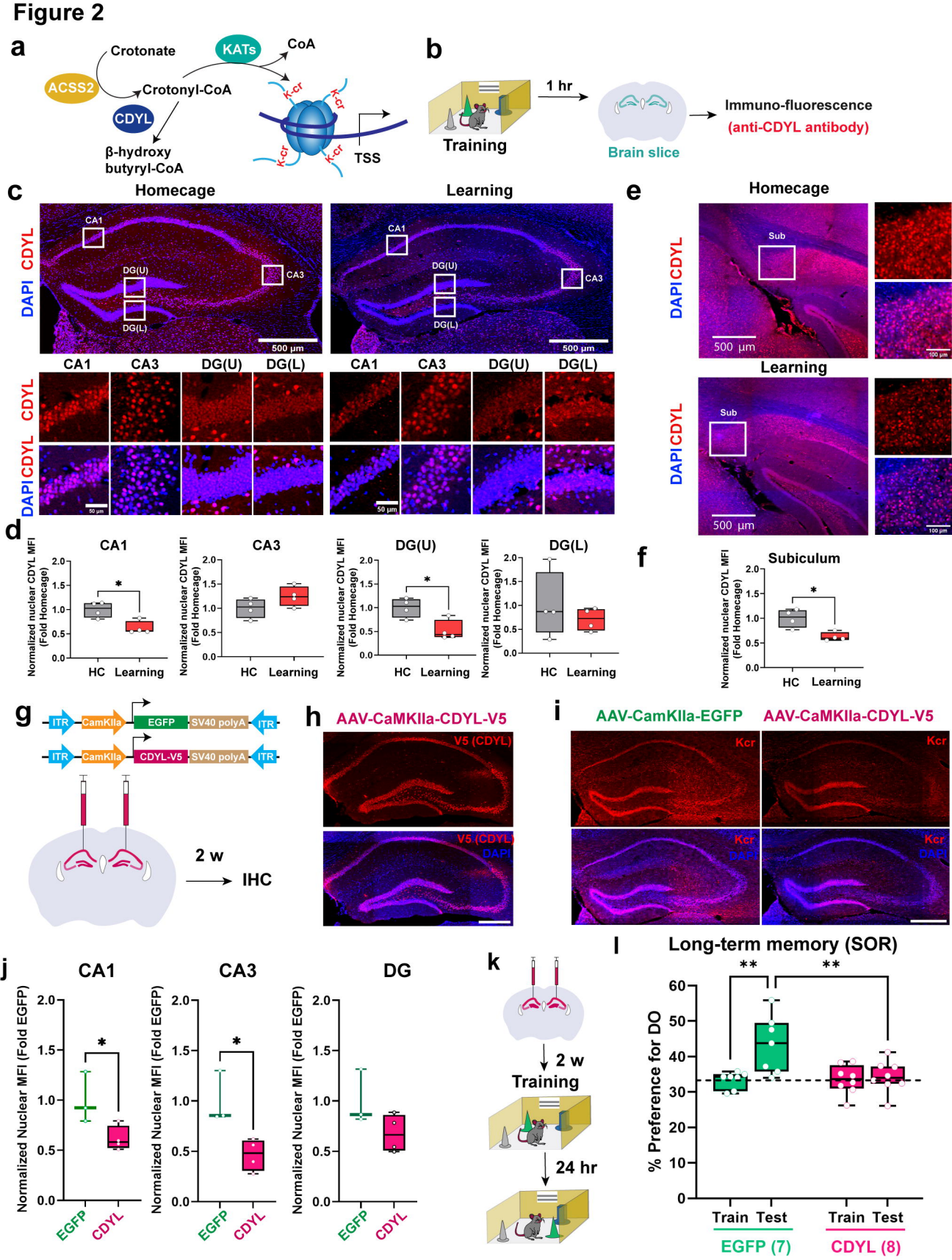
Figure 2
a
Crotonate
KATs
CoA
ACSS2
Crotonyl-CoA
CDYL
β-hydroxy butyryl-CoA
K-cr
TSS
b
1 hr
Training
Brain slice
Immuno-fluorescence
(anti-CDYL antibody)
c
Homecage
Learning
CA1
CA3
DG(U)
DG(L)
DAPI CDYL
500 μm
50 μm
d
CA1
CA3
DG(U)
DG(L)
Normalized nuclear CDYL MFI (Fold Homecage)
HC
Learning
e
Homecage
Learning
Sub
500 μm
100 μm
f
Subiculum
g
ITR
CamKIIa
EGFP
SV40 polyA
CDYL-V5
2 w
IHC
h
AAV-CaMKIIa-CDYL-V5
V5 (CDYL)
DAPI
i
AAV-CamKIIa-EGFP
AAV-CaMKIIa-CDYL-V5
Kcr
j
CA1
CA3
DG
Normalized Nuclear MFI (Fold EGFP)
EGFP
CDYL
k
2 w
Training
24 hr
l
Long-term memory (SOR)
% Preference for DO
Train Test
EGFP (7)
CDYL (8)

Figure 3

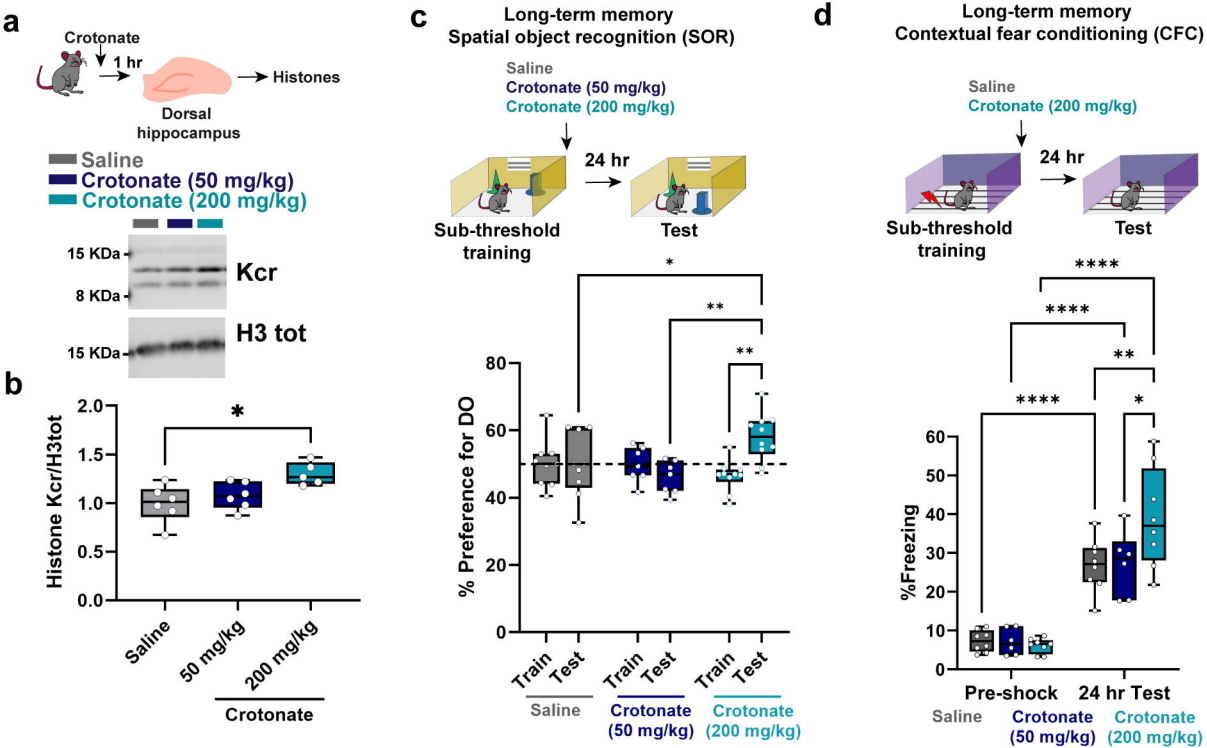
a
Crotonate
1 hr
Histones
Dorsal hippocampus
Saline
Crotonate (50 mg/kg)
Crotonate (200 mg/kg)
15 KDa
8 KDa
Kcr
15 KDa
H3 tot
b
Histone Kcr/H3tot
2.0
1.5
1.0
0.5
0.0
*
Saline
50 mg/kg
200 mg/kg
Crotonate
c
Long-term memory
Spatial object recognition (SOR)
Saline
Crotonate (50 mg/kg)
Crotonate (200 mg/kg)
24 hr
Sub-threshold training
Test
% Preference for DO
80
60
40
20
0
*
**
**
Train
Test
Train
Test
Train
Test
Saline
Crotonate (50 mg/kg)
Crotonate (200 mg/kg)
d
Long-term memory
Contextual fear conditioning (CFC)
Saline
Crotonate (200 mg/kg)
24 hr
Sub-threshold training
Test
%Freezing
60
50
40
30
20
10
0
****
****
**
****
*
Pre-shock
24 hr Test
Saline
Crotonate (50 mg/kg)
Crotonate (200 mg/kg)

Figure 4

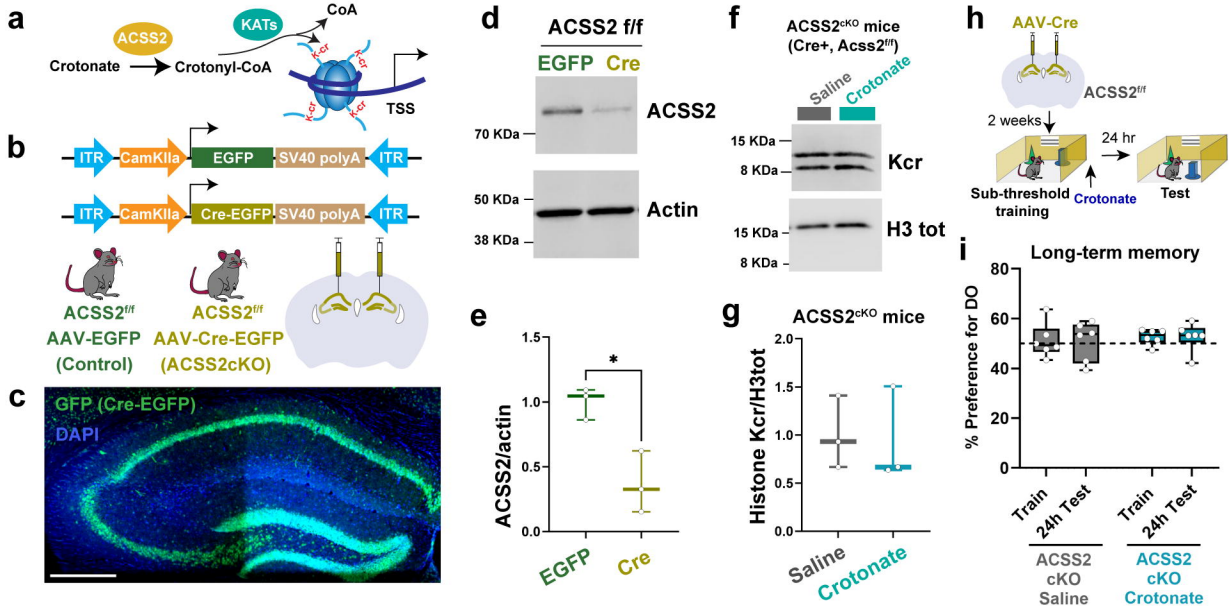
a
ACSS2
KATs
CoA
Crotonate
Crotonyl-CoA
Kcr
TSS
b
ITR
CamKIIa
EGFP
SV40 polyA
ITR
ITR
CamKIIa
Cre-EGFP
SV40 polyA
ITR
ACSS2f/f
AAV-EGFP
(Control)
ACSS2f/f
AAV-Cre-EGFP
(ACSS2cKO)
c
GFP (Cre-EGFP)
DAPI
d
ACSS2 f/f
EGFP
Cre
70 KDa
ACSS2
50 KDa
Actin
38 KDa
e
ACSS2/actin
1.5
1.0
0.5
0.0
*
EGFP
Cre
f
ACSS2cKO mice
(Cre+, Acss2f/f)
Saline
Crotonate
15 KDa
8 KDa
Kcr
15 KDa
8 KDa
H3 tot
g
ACSS2cKO mice
Histone Kcr/H3tot
2.0
1.5
1.0
0.5
0.0
Saline
Crotonate
h
AAV-Cre
ACSS2f/f
2 weeks
24 hr
Sub-threshold
training
Crotonate
Test
i
Long-term memory
% Preference for DO
80
60
40
20
0
Train
24h Test
Train
24h Test
ACSS2
cKO
Saline
ACSS2
cKO
Crotonate

Figure 5

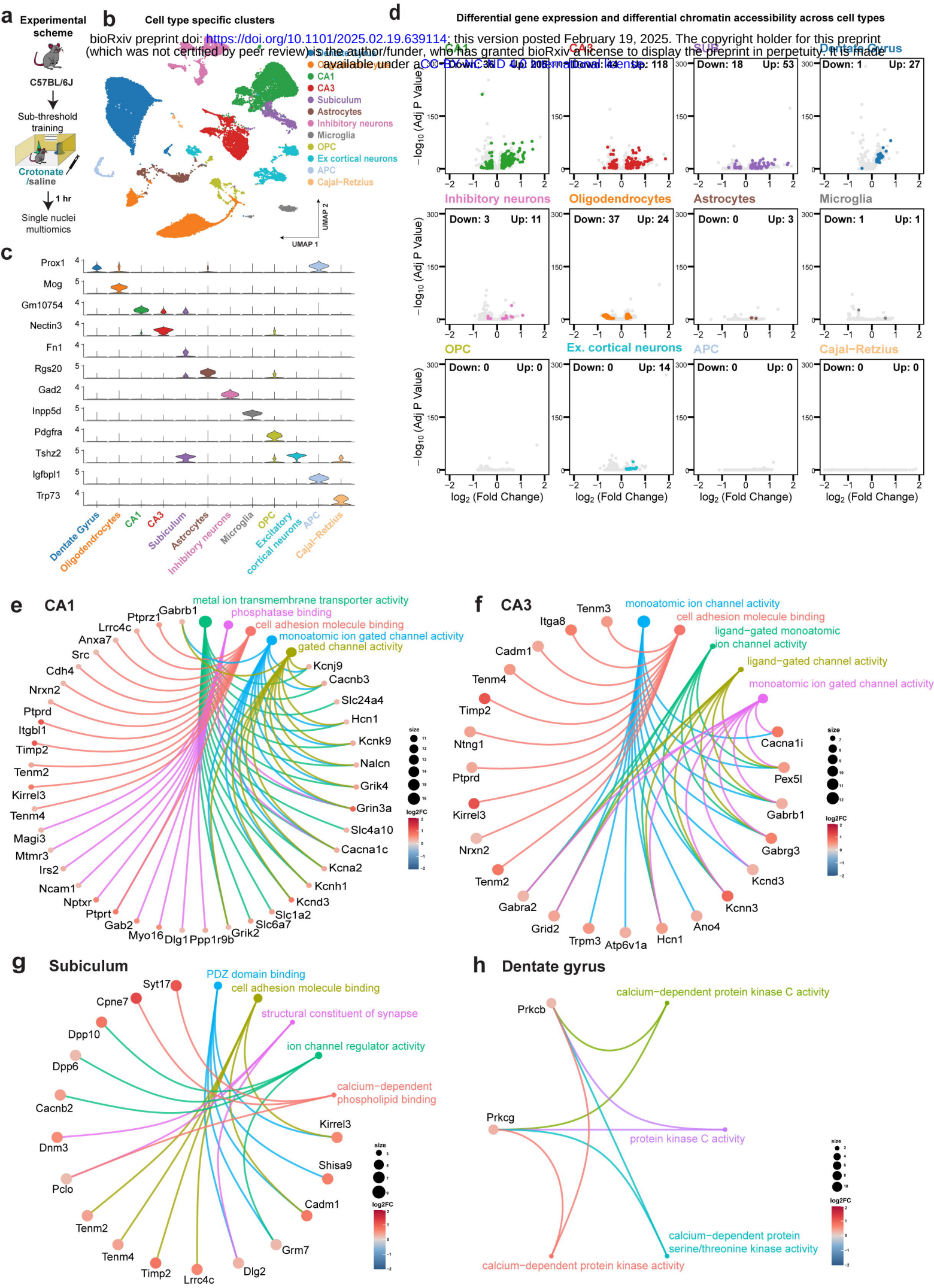

Figure 6